Numerical analysis of a turbocharger compressor

Kristaq Hazizi[1,*], *Ahad* Ramezanpour[2], *Aaron* Costall[3], and *Mehrdad* Asadi[4]

[1,2,4]Faculty of Science & Technology, Anglia Ruskin University, Chelmsford CM1 1SQ, UK
[3]Mechanical Engineering Department, Imperial College London, London SW7 2AZ, UK
[*]Faculty of Science & Technology, Anglia Ruskin University, Chelmsford CM1 1SQ, UK:
Email: kristaq.hazizi@pgr.anglia.ac.uk

Abstract. The automotive industry is under obligation to meet regulations for emission control that has resulted in further use of turbochargers in passenger cars to enable downsizing and increase engine power density. In this study, a set of numerical simulations are conducted along two turbocharger compressor speed lines of 150,000 rpm and 80,000 rpm to analyse and validate the results against experimental data. The domain includes the full compressor stage comprising intake, impeller as a Multiple Reference Frame, diffuser and outlet. The k-omega SST turbulence model with three different mesh sizes is used to solve the compressible flow using ANSYS Fluent software. Three points on each speed-line are selected: one point each in regions close to surge and choke and a point in the stable zone of the compressor map. The simulations predict compressor performance in terms of the total-to-total pressure ratio and total-to-total efficiency. Results reveal the predicted pressure ratio error is in the range of 1-6%. At 150,000 rpm the pressure ratio is underpredicted for the point close to the surge but overpredicted for the point close to the choke. However, the pressure ratio results are within 1% difference for 80,000 rpm. In all cases, the predicted efficiency increased when a finer mesh is used. While results are close to the experimental data in both the surge and stable areas of the map, the efficiency was overpredicted up to 20% in the region close to the choke. In conclusion, the finer mesh leads to higher pressure ratio and efficiency values that overpredict the performance, especially for the point close to choke.

Keywords: Turbocharger compressor, CFD, k-ω SST turbulence model, Compressor performance.

1. Introduction and literature review

The turbocharger compressor has an irreplaceable role in improving engine power, reducing fuel consumption and decreasing emissions. Because of geometrical complexity, time and labour adopting experiments to gain relevant experimental data, it becomes more economical to simulate turbocharger compressor internal flow field and study numerical analysis data.

The purpose of this paper is to develop and analyses a numerical model of the selected turbocharger compressor passenger car using ANSYS Fluent as commercial CFD code and validate the results with experimental data at two different rotational speeds.

Abdelmadjid, Mohamed and Boussad (2013) [1] showed that volute geometry has a considerable impact on the pressure and temperature values at the compressor outlet. Three different volute designs with same impeller and diffuser were numerically analysed at 100,000 rpm with steady conditions and compared with each other. Effects of the shape of the volute cross section and the location of the volute inlet on overall performance and operating range are investigated.

In the study of Baris and Mendonça (2012) [2] turbocharger compressor performance characteristics between 100,000 and 200,000 rpm values were investigated numerically in steady state and compared with rig measurements. Polyhedral volume mesh was used with tetrahedral boundary layer mesh in the entire flow model and turbulence was modelled with the k-omega SST model. The total pressure and total temperature were applied as inlet boundary condition and static pressure was applied as outlet condition. Numerical results accuracy level is achieved within 2% difference of rig measurements.

ÇANGA (2016) [3] compared CFD simulations and test results of a turbocharger compressor in their study. Compressor performance map is created by tests performed between 60,000 and 150,000 rpm rotational speed values. On the other hand, CFD studies are carried out for four different operating conditions at 120,000 rpm. Numerical results showed better similarity with test results at low flow rate values, while deviation is increased at higher flow rates.

Some fundamental data of characteristics of the fluid should be known such as: pressure ratio π, temperature of the fluid, volumetric flow rate q_v and either the polytrophic efficiency η_p or the isentropic efficiency η_s of the compression process (Essi Paavilainen, 2008) [4].

In the numerical study of (Jawad *et al.*, 2013) [5], the effect of double splitters on a modified turbocharger compressor performance is investigated. The polyhedral mesh structure is used for volume mesh generation and turbulence is modelled with k-ω-SST model. Total pressure and total temperature boundary condition are set at the inlet and static pressure is set at the outlet. The parametric simulations showed that the potential of double splitter in improving centrifugal compressor performance.

Kalinkevych and Shcherbakov (2013) [6] investigated the flow phenomena in a vaneless diffuser of a centrifugal compressor stage experimentally, numerically and analytically. In the analytical investigations, the time-averaged boundary layer parameters have been considered. Furthermore, two boundary regions have been used; one with laminar flow and the other with turbulent flow. It has been found from the numerical analysis that there is an average difference of 17.3% and 14.5% in total pressure loss coefficient in predicted and measured results. Moreover, the average difference between the measured and predicted static pressure recovery coefficients is 2.3% and 4.7%. The investigations show that at low mass flow rates, the pressure losses are caused by the flow separation close to the diffuser hub wall. It is due to the higher frictional losses and jet wake mixing. Similarly, at high flow rates, the pressure losses are only caused by the jet wake mixing.

The operating principle and the theory on the determination of the flow that passes through the compressor and isentropic compression efficiency is very complex (Mokhatab, Poe and Mak, 2018) [7].

The turbocharger compressor geometry has been the subject of numerous mathematical and numerical studies as it strongly affects the overall performance, stability, operating range and the location of the best efficiency point of the compressor (Soliman *et al.*, 2018) [8].

Pressure ratio and the isentropic efficiency are two main performance characteristics of a turbocharger compressor. This investigation is about a turbocharger compressor stage composed of casing, diffuser, and impeller. Three different mesh size cases are selected, three operation points for each speed-line of 80,000 rpm and 150,000 rpm, are solved and numerical results obtained for the purpose of validation.

The results obtained from CFD analysis compared with the experimental data. Considering wide use of these turbocharger compressors, the impact of the research on improving power density, downsizing the engine with the same performance, is invaluable in increasing fuel efficiency and decreasing emissions. Furthermore, the turbocharger compressors reduced in size and improving efficiency could be used for new applications and open optimisation routes in a variety of other products.

2. Governing equations

2.1. Reynolds Averaged Navier-Stokes Equations

This study involves the use of experiment and observations to measure possible outcomes by computer simulations and use mathematical techniques to process and manipulate the measured quantities for validation purposes.

The Reynolds Averaged Navier-Stokes (RANS) equations describe the statistic average component of turbulent flows; the instantaneous turbulent field is conventionally decomposed into an average component and a fluctuating component of zero average. For a

steady-state compressible flow, these equations are more specifically denoted as Favre averaged NS equations.

Three essential equations are solved for in ANSYS Fluent in order to capture the flow characteristics and its evolution through the compressor. They are called the governing equations in the subject of fluid mechanics and are the steady Navier-Stokes equations. The Navier-Stokes equations are the conservation of mass (continuity), the conservation of momentum, and the conservation of energy, and are defined below in cartesian tensor notation presented in the following form:

2.1.1. *Continuity equation:*

$$\frac{\partial \rho}{\partial t} + \frac{\partial(\rho u_i)}{\partial x_i} = 0 \; ; \qquad (1)$$

2.1.2. *Momentum equation:*

$$\frac{\partial}{\partial x_i}(\rho u_i u_j) = -\frac{\partial P}{\partial x_i} + \frac{\partial}{\partial x_j}\left[\mu\left(\frac{\partial u_i}{\partial x_i} + \frac{\partial u_j}{\partial x_i} - \frac{2}{3}\delta_{ij}\frac{\partial u_m}{\partial x_m}\right)\right] + \frac{\partial}{\partial x_j}\left[\mu_t\left(\frac{\partial u_i}{\partial x_j} + \frac{\partial u_j}{\partial x_i}\right) - \frac{2}{3}\left(\rho k + \mu_t \frac{\partial u_m}{\partial x_m}\right)\delta_{ij}\right]; \qquad (2)$$

Where ρ represents the density (kgm^3), u the velocity (ms^1), P the pressure (Pa), k the turbulence kinetic energy ($m^2\ s^{-2}$), μ the laminar viscosity ($kgm^{-1}s^{-1}$), and μ_t the turbulent viscosity ($kgm^{-1}s^{-1}$). The subscripts i, j and m represent the directions x, y, and z. The symbol δij is the Kronecker delta, it is 1 when i = j, otherwise it is 0.

2.1.3. *Energy equation:*

$$(\tau_{ij})_{eff} = (\mu + \mu_t)\left(\frac{\partial u_i}{\partial x_j} + \frac{\partial u_j}{\partial x_i} - \frac{2}{3}\delta_{ij}\frac{\partial u_m}{\partial x_m}\right); \qquad (3)$$

Where $(\tau_{ij})_{eff}$ = viscous stress tensor ($kgm^{-1}\ s^{-2}$).

2.1.4. *k-omega Turbulence model:*

The eddy viscosity Vt, is written as: Vt = k/ω and P, is written as: $P = \tau_{ij}\frac{\partial u_i}{\partial x_j}$; instead the generation of k and omega is presented as follows:

$$\frac{\partial(\rho k)}{\partial t} + \frac{\bar{\partial}(\rho u_j k)}{\partial x_j} = \rho P - \beta^* \rho \omega k + \frac{\partial}{\partial x_j}\left[\left(\mu + \sigma_k \frac{\rho k}{\omega}\right)\frac{\partial k}{\partial x_j}\right]; \qquad (4)$$

$$\frac{\partial(\rho\omega)}{\partial t} + \frac{\partial(\rho u_j \omega)}{\partial x_j} = \frac{\gamma\omega}{k} P - \beta\rho\omega^2 + \frac{\partial}{\partial x_j}\left[\left(\mu + \sigma_\omega \frac{\rho k}{\omega}\right)\frac{\partial \omega}{\partial x_j}\right] + \frac{\rho\sigma_d}{\omega}\frac{\partial k}{\partial x_j}\frac{\partial \omega}{\partial x_j}\; ; \qquad (5)$$

3. Numerical setting

2.2. The Compressor Geometry

An initial geometry is supplied from industrial collaboration Mitsubishi and Engine Europe (MTEE). The various components of the compressor are constructed individually performing further elaboration of checking, cleaning and editing the complex geometry and then extracting the fluid domain. The fluid domain geometry consists of three parts, namely the inlet, impeller and outlet. A full domain CAD is completed as shown in **Figure 1** to allow for accurate and comprehensive CFD results.

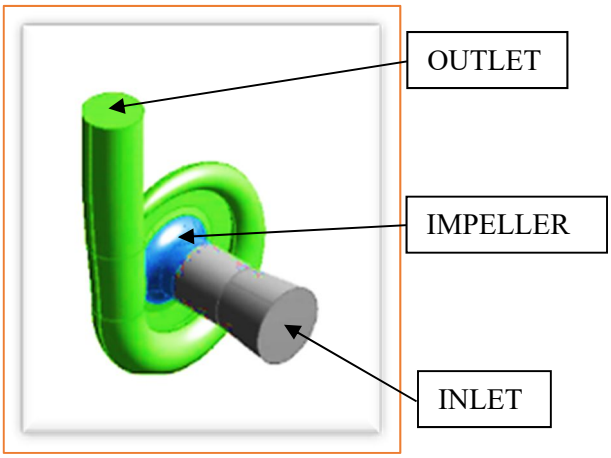

Figure 1 Fluid Domain

2.3. Meshing

In simulation fields, grid numbers and distribution have a great influence on the results. Irrationality of grid distribution and number may lead to bad results, and too many grids may need a long time to get results. Thus, to obtain a suitable grid number grade, we study the influences of grid number to the numerical calculation results.

Besides turbo knowledge, a big part of CFD simulation demands high precision in meshing to avoid errors. For that reason, a mesh study is great importance and the use of a mesh study is a way to prove the reliability of the mesh.

Taking into consideration that the mesh size must be kept small in order to complete the simulations in a reasonable time. However, a coarser mesh could negatively affect the accuracy of the results.

Given the complexity of the compressor geometry, the full computational domain is meshed with tetrahedral grid cells, the clearance gap between the impeller and the diffuser is taken into consideration when meshing the impeller volume, near the impeller blade and diffuser vane walls.

A grid dependence study is carried out to guarantee that the numerical solutions are grid-dependent. Hence, a fine grid size of elements is used for the computational

fluid dynamic calculation reported in this paper respectively, 3 different mesh size cases of 2, 3 and 5 Million of mesh elements have been used throughout all the simulations.

The mesh is refined, as shown in **Figure 2**.

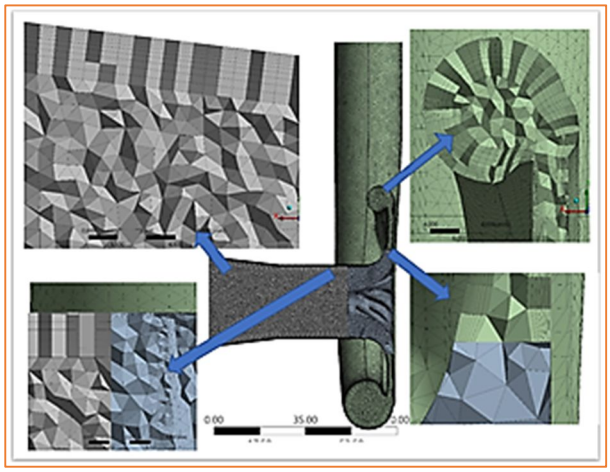

Figure 2 Fluid Domain Mesh Cut-Section

4. Fluent setting

The numerical investigations are carried out using a commercial CFD code, ANSYS Fluent. The three-dimensional model of centrifugal compressor along with its fluid domain is created. Unstructured tetrahedral elements are used for grid generation within the domain and tetrahedral prism used close to the walls. Boundary conditions, solver parameters, convergence criteria are defined, and a numerical model is developed.

Numerical studies are conducted in steady-state conditions with pressure ratio inlet and mass flow rate as the outlet boundary conditions for the operating points 24, 23, 8 and 10. Instead, the operating points 27 and 13 have used mass flow rate inlet and pressure ratio outlet as boundary conditions. Points 8, 13, 23, 27 are closes points to surge and choke that could be modelled using steady state model in this study **(Table 1)**.

Besides, the rotation of compressor wheel modelled with rotating (moving) multiple reference frame method while k-omega SST turbulence model is used to solve compressible flow. Governing equations include Navier Stokes equations, energy equation, and two equations for turbulence including turbulence kinetic energy (k) and specific dissipation rate (omega). The convergence of the solutions was monitored by creating surface goals for density, total to total pressure, mass and volumetric flow rates at the outlet of the compressor.

CFD preliminary results are been post-processed for any errors or shortcomings, adjustments and modifications made before the final calculations being obtained.

The numerical model is solved until the defined convergence criteria is reached and results are obtained as shown in **Figure 3**.

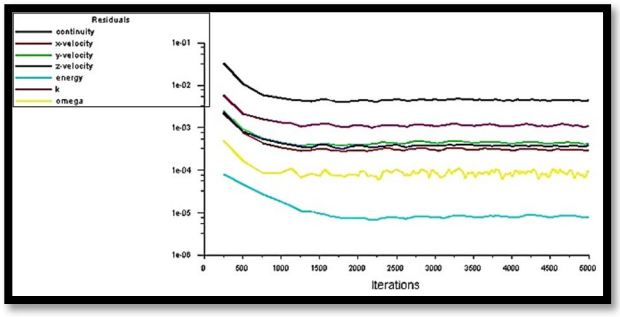

Figure 3 Typical Error Residuals

5. Results and discussions

Obtained numerical solutions are compared with each other and validated with experimental results for analysis.

Table 1 shows the list of points for both speed lines along with the pressure ratio results for various mesh numbers compared to the experimental data.

Table 1 Numerical Results of Pressure Ratio

Pressure Ratio					
Points	**Mesh Number** (Million)			**Exp. data**	**Speed** (rpm)
	2	3	5		
8 (Close to Surge)	1.18	1.18	1.19	1.17	80,000
10 (Central)	1.14	1.14	1.15	1.15	80,000
13 (Close to Choke)	1.06	1.07	1.07	1.07	80,000
23 (Close to Surge)	1.66	1.68	1.68	1.70	150,000
24 Central)	1.55	1.60	1.62	1.65	150,000
27 (Close to Choke)	1.28	1.30	1.31	1.25	150,000

The predicted pressure ratio of the simulation results achieved for the operating points 23, 24 and 27, speed line 150,000 (rpm) are shown in graph **Figure 4**. The same results for the operating points 8, 10 and 13, speed line 80,000 (rpm) are shown on graph **Figure 5.**

From the comparison between different numerical pressure ratios results at both speed lines versus experimental data, it can be observed that:

- Pressure ratio for operating point 13 (choke area) is underpredicted in mesh size case of 2 Million and overpredicted in other mesh size cases.
- Pressure ratio for operating points 27 (Choke area) and 8 (Surge area) is overpredicted in all mesh size cases.

- Pressure ratio for operating points 24, 10 (Central area) and 23 (Surge area) is underpredicted in all mesh size cases.

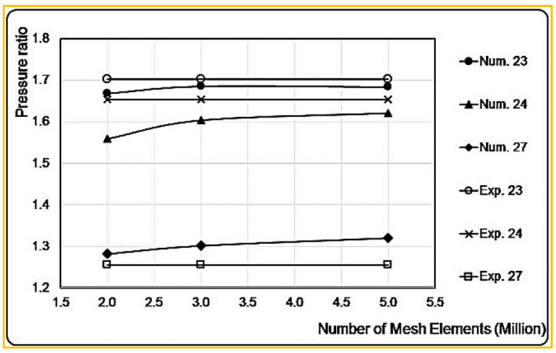

Figure 4 Pressure Ratio at 150,000 rpm

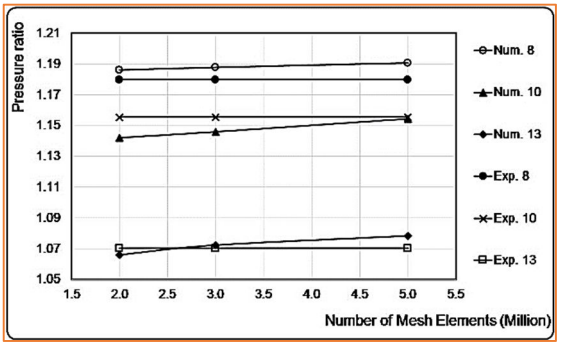

Figure 5 Pressure Ratio at 80,000 rpm

Table 2 shows the list of points for both speed lines along with the efficiency results for various mesh numbers compared to the experimental data.

Table 2 Numerical Results of Efficiency

Efficiency					
Points	**Mesh Number** (Million)			**Exp. data**	**Speed** (rpm)
	2	3	5		
8 (Close to Surge)	0.70	0.69	0.72	0.65	80,000
10 (Central)	0.73	0.76	0.79	0.72	80,000
13 (Close to Choke)	0.47	0.52	0.56	0.47	80,000
23 (Close to Surge)	0.70	0.72	0.74	0.72	150,000
24 Central)	0.72	0.76	0.78	0.77	150,000
27 (Close to Choke)	0.50	0.54	0.57	0.47	150,000

Predicted efficiency of the simulation results achieved for the operating points 23, 24 and 27, speed line 150,000 (rpm) are shown in graph **Figure 6.** The same results for the operating points 8, 10 and 13, speed line 80,000 (rpm) are shown on graph **Figure 7.**

From the comparison between different numerical efficiency results at both speed lines versus experimental data, it can be observed that:

- Efficiency for operating points 27 (Choke area), 10 (Central area) and 8 (Surge area) is overpredicted in all mesh size cases.
- Efficiency operating points 24 (Central area) and 23 (Surge area) is overpredicted in mesh size case of 5 Million and underpredicted for other mesh size cases.
- Efficiency operating point 13 (Choke area) is overpredicted in mesh size cases 3 and 5 Million.

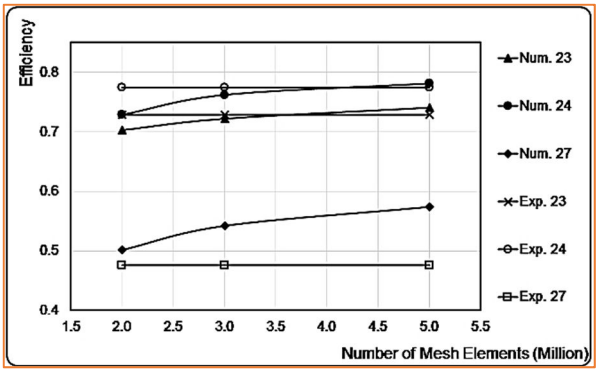

Figure 6 Efficiency at 150,000 rpm

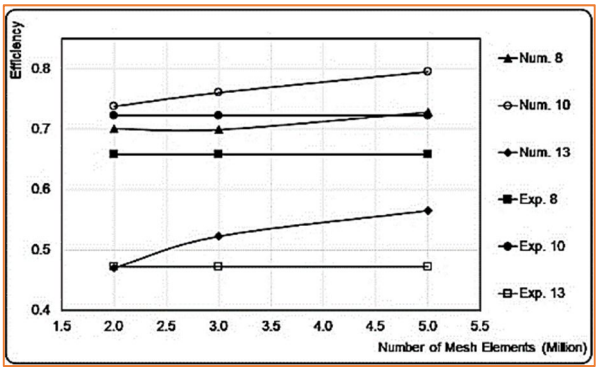

Figure 7 Efficiency at 80,000 rpm

Table 3 shows the list of points for both speed lines along with the pressure ratio error percentage results for various mesh numbers compared to the experimental data.

Table 3 Numerical Results of Pressure Ratio Error

Pressure Ratio Error (%)				
Points	**Mesh Number** (Million)			**Speed** (rpm)
	2	3	5	
8 (Close to Surge)	-0.5	-0.6	-0.92	80,000
10 (Central)	1.1	0.8	0.10	80,000
13 (Close to Choke)	0.3	-0.2	-0.78	80,000
23 (Close to Surge)	2.0	1.0	1.10	150,000
24 Central)	5.6	2.9	1.92	150,000
27 (Close to Choke)	-2.12	-3.65	-5.11	150,000

Predicted pressure ratio percentage error of the simulation results achieved for the operating points 23, 24 and 27, speed line 150,000 (rpm) are shown on the graph **Figure 8**. The same results for the operating points 8, 10 and 13, speed line 80,000 (rpm) are shown on the graph **Figure 9**.

From the comparison between different numerical pressure ratios results at both speed lines versus experimental data, it can be observed that:

- Pressure ratio error for operation points 24, 10 (Central area) and 23 (Surge area) is overpredicted in all mesh size cases.
- Pressure ratio error for operation point 27 (Choke area) and 8 (surge area) is underpredicted in all mesh size cases.
- Pressure ratio error for operation point 13 (Choke area) is overpredicted for mesh size case of 2 Million and underpredicted for other mesh size cases.

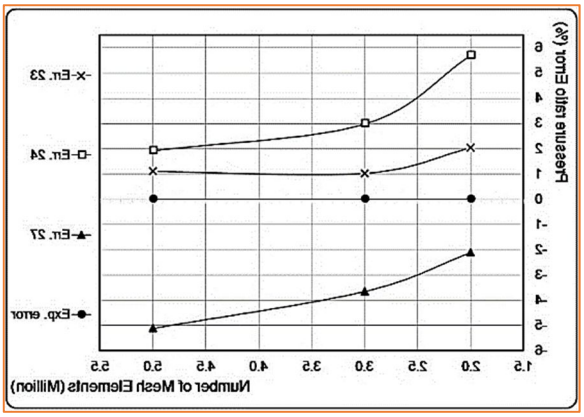

Figure 8 Pressure Ratio Error at 150,000 rpm

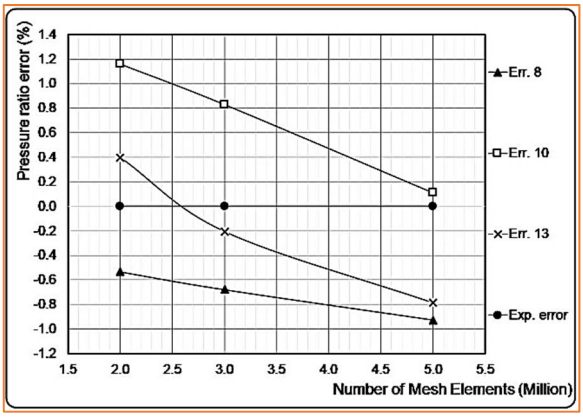

Figure 9 Pressure Ratio Error at 80,000 rpm

Table 4 shows the list of points for both speed lines along with the efficiency percentage error results for various mesh numbers compared to the experimental data.

Table 4 Numerical Results of Efficiency Error

Efficiency Error (%)				
Points	**Mesh Number** (Million)			**Speed** (rpm)
	2	3	5	
8 (Close to Surge)	-6.4	-6.2	-10.6	80,000
10 (Central)	-2.0	-5.2	-10.0	80,000
13 (Close to Choke)	0.5	-10.5	-19.6	80,000
23 (Close to Surge)	3.5	0.8	-1.6	150,000
24 Central)	5.8	1.5	-0.9	150,000
27 (Close to Choke)	-5.5	-14.0	-20.7	150,000

Predicted efficiency percentage error of the simulation results achieved for the operating points 23, 24 and 27, speed line 150,000 (rpm) are shown in graph Figure 10. The same results for the operating points 8, 10 and 13, speed line 80,000 (rpm) are shown on the graph.

From the comparison between different numerical efficiency percentage error results at both speed lines versus experimental data, it can be observed that:

- Efficiency percentage error for operation point 13 (Choke area) is overpredicted in mesh size case of 2 Million and underpredicted in other mesh size cases.
- Efficiency percentage error for operation points 24 (Central area), and 23 (Surge area) is underpredicted for mesh size case of 5 Million and overpredicted for other mesh size cases.
- Efficiency percentage error for operation points 27 (Choke area), 8 (Surge area) and 10 (Central area) are underpredicted in all mesh size cases.

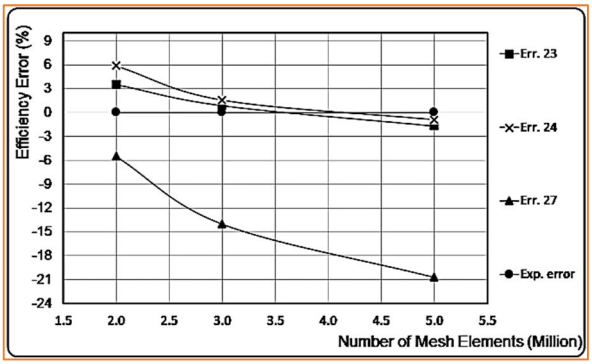

Figure 10 Efficiency Error at 150,000 rpm

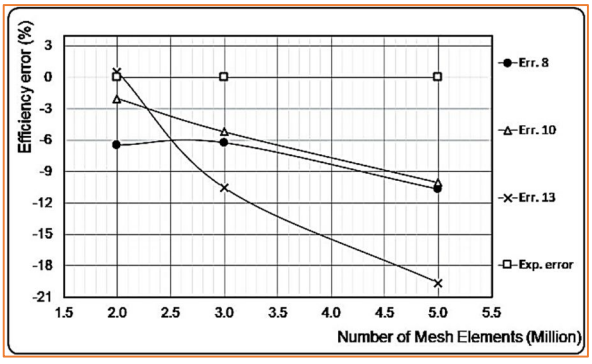

Figure 11 Efficiency Error at 80,000 rpm

6. Conclusion

This paper presents an effort to model the flow from the inlet to the exit of a turbocharger compressor stage consisting of all the components in place and performance prediction by providing numerical analysis using CFD tools and these are verified by experimental data.

A good agreement was achieved between the computational fluid dynamics (CFD), calculated and the experimental results, on the isentropic efficiency of a centrifugal compressor stage with maximum variation in operating point 27 (Choke area).

As well as the total pressure ratio of a centrifugal compressor stage as estimated by CFD tools almost complies, with negligible maximum variation in operating point 24 (Central area).

For the isentropic efficiency error of a centrifugal compressor, stage reaches a maximum variation of 20%. For the total pressure ratio error of a centrifugal compressor, stage reached an estimated maximum variation of 6%.

The finer mesh at both speed lines leads in decreasing pressure ratio error values that overpredict the performance, especially for points close to the central area and increasing pressure ratio error values that underpredict the performance, especially for the points close to choke. Instead for efficiency error at both speed lines the finer mesh lead in increasing efficiency error values that underpredict the performance, especially for the points close to surge.

Acknowledgments:

I wish to express my greatest appreciation to my supervisors Dr. Ahad Ramezanpour and Dr. Aaron Costal for their useful suggestions and worthy discussions about this work guidance throughout my research and I would like to thank for the industrial collaboration Mitsubishi Turbocharger and Engine Europe (MTEE) for providing the compressor geometry and test data.

References

1. Abdelmadjid, C., Mohamed, S. A. and Boussad, B. (2013) ‘CFD analysis of the volute geometry effect on the turbulent air flow through the turbocharger compressor’, in *Energy Procedia*. Elsevier Ltd, pp. 746–755. doi: 10.1016/j.egypro.2013.07.087.
2. Baris, O. and Mendonça, F. (2012) ‘Automotive Turbocharger Compressor CFD and Extension Towards Incorporating Installation Effects’, in. ASME International, pp. 2197–2206. doi: 10.1115/gt2011-46796.
3. ÇANGA, Z. (2016) *Theorical and Experimental Analysis of Turbocharger in Tractor Engine*.
4. Essi Paavilainen (2008) ‘Seminar in energy technology The performance and the characteristic field of a centrifugal compressor’.
5. Jawad, L. H. *et al.* (2013) ‘Numerical investigation on the effect of impeller trimming on the performance of a modified compressor’, *CFD Letters*, 5(4), pp. 174–184.
6. Kalinkevych, M. and Shcherbakov, O. (2013) ‘Numerical Modeling of the Flow in a Vaneless Diffuser of Centrifugal Compressor Stage’, *ISRN Mechanical Engineering*. Hindawi Limited, 2013, pp. 1–9. doi: 10.1155/2013/602384.
7. Mokhatab, S., Poe, W. A. and Mak, J. Y. (2018) ‘Natural Gas Compression’, in *Handbook of*

Natural Gas Transmission and Processing. Elsevier, pp. 433–461. doi: 10.1016/b978-0-12-815817-3.00014-9.

8. Soliman, M. *et al.* (2018) 'Modeling and CFD Analysis of Air Flow through Automotive Turbocharger Compressor: Analytical Approach and Validation', *Journal of Engineering Science and Military Technologies*. Egypts Presidential Specialized Council for Education and Scientific Research, 17(17), pp. 1–15. doi: 10.21608/ejmtc.2017.21597.